Solid-State Electronics Vol. 21, pp. 1109–1117

0038-1101/78/0901-1109/$02.00/0

THE DOPANT DENSITY AND TEMPERATURE DEPENDENCE OF HOLE MOBILITY AND RESISTIVITY IN BORON DOPED SILICON†

SHENG S. LI

Department of Electrical Engineering, University of Florida, Gainesville, FL 32611, U.S.A.

(*Received* 14 *October* 1977; *in revised form* 15 *March* 1978)

Abstract—Theoretical expressions for computing resistivity and conductivity mobility of holes as functions of dopant density and temperature have been derived for boron-doped silicon. The model is applicable for dopant densities from 10^{13} to $3\times10^{18}\,cm^{-3}$ and temperatures between 100 and 400 K.

Using a 3-band [i.e. heavy-hole, light-hole and the spin–orbit splitting (SO) band] model, the hole mobility was calculated by properly combining the contributions from scattering by lattice phonons, ionized impurities and neutral impurities. In addition, the effects of hole–hole (h–h) scattering and nonparabolicity of valence bands were taken into account in the mobility formulation.

To verify our theoretical calculations, resistivity measurements on nine boron-doped silicon slices with dopant densities from 4.5×10^{14} to $3.2\times10^{18}\,cm^{-3}$ were performed for $100\le T\le400$ K, using planar square-array test structure. Agreement between our calculated and measured resistivity values was within 6 percent over the entire range of dopant density and temperature studied here. Excellent agreement (within ±5%) between our calculated hole mobility values and those of Wagner[9] was obtained for $N_A\le10^{17}\,cm^{-3}$ for boron-doped silicon, while discrepancies were found for boron densities greater than $10^{17}\,cm^{-3}$. This discrepancy is attributed to neglecting the effect of deionization of boron impurities at higher dopant densities by Wagner (i.e. assuming hole density is equal to the total boron density).

NOTATION

Unless stated otherwise, all units are in MKS.

E	energy of holes
E_A	acceptor energy level
E_F	Fermi energy level
E_g	energy band gap
E_N	binding energy of neutral acceptors
E_V	valence band edge
h	Planck's constant ($=6.625\times10^{-34}$), $\hbar=h/2\pi$
k	Boltzmann's constant, $=1.38\times10^{-23}$
m_0	free electron mass, $=9.1\times10^{-31}$
m^*_{C1}	conductivity effective mass in heavy hole band, in units of m_0
m^*_{C2}	conductivity effective mass in light-hole band
m^*_{C3}	conductivity effective mass in spin–orbit-splitting (SOS) band
m^*_{D1}	density of states effective mass in heavy-hole band
m^*_{D2}	density of states effective mass in light-hole band
m^*_{D3}	density of states effective mass in SOS band
m^*_D	total density of states effective mass of hole
N_A	total boron density, cm^{-3}
N_A^-	ionized boron density, cm^{-3}
N_N	neutral boron density, cm^{-3}
N_v	effective density of valence band states, cm^{-3}
p	hole density, cm^{-3}
p'	effective screening hole density, cm^{-3}
q	electronic charge, $=1.6\times10^{-19}$
T	absolute temperature, K
ϵ_0	free space permittivity, $=8.854\times10^{-12}$
ϵ_s	permittivity of silicon, $=11.7\times\epsilon_0$
μ_L	lattice scattering mobility of holes, $cm^2/V\cdot S$
μ_I	ionized impurity scattering mobility, $cm^2/V\cdot S$
μ_N	neutral impurity scattering mobility, $cm^2/V\cdot S$
μ_{LI}	combined lattice and ionized impurity scattering mobility, $cm^2/V\cdot S$
μ_p	total hole conductivity mobility, $cm^2/V\cdot S$
τ	relaxation time, sec.
ρ	resistivity of holes, $\Omega\cdot cm$.

†This research was supported in part by the Advanced Research Projects Agency Order No. 2397 through the National Bureau of Standards' Semiconductor Technology Program Contract No. 7-35741 and in part by the National Science Foundation Grant No. ENG 76-81828.

1. INTRODUCTION

Although a considerable amount of work on mobility and resistivity in p-type silicon has been published[1–10], due to the complexity of the valence band structure and of the various scattering mechanisms involved, only limited success has been achieved in the mobility calculations. For example, Ottaviani *et al.*[1] have developed a microscopic theoretical model applicable only to computation of ohmic mobility in high purity p-type silicon in which nonpolar optical and acoustical phonon scattering is dominant. In their theoretical analysis, they have shown the necessity of considering band nonparabolicity in mobility formulation, and have pointed out the band warping effect to be secondary in importance to that of nonparabolicity. The lattice mobilities for holes in p-type silicon are well established for temperatures between 50 and 400 K[1–6]. Braggins[4] has analyzed carrier concentration and hole mobility in boron-doped silicon from Hall effect and resistivity measurements. Using a three-band model and relaxation time approximation, his calculations of impurity densities appear to agree well with Hall effect data for boron densities less than $5\times10^{16}\,cm^{-3}$. In spite of the fact that large discrepancies exist among the published hole mobility data[8–10] for dopant densities greater than $10^{16}\,cm^{-3}$, no adequate theoretical model is available for mobility and resistivity calculations in p-type silicon that

is valid over a wide range of dopant densities and temperatures.

The purpose of this paper is to present our theoretical and experimental investigations of the dopant density and temperature dependence of hole mobility and resistivity in boron-doped silicon for $10^{13} \leq N_A \leq 3 \times 10^{18}\,\text{cm}^{-3}$ and $100 \leq T \leq 400\,\text{K}$.

To overcome difficulties in effective mass calculations and mobility formulation the valence band structure of silicon was approximated by a three-band model consisting of a spherical, parabolic heavy-hole band, a spherical, nonparabolic light-hole band, and a spherical, parabolic spin–orbit band[11]. Together with this model, the relaxation time approximation was used to develop theoretical expressions for mobility of holes in p-type silicon. Scattering mechanisms due to lattice (i.e. acoustical and optical phonons), ionized impurity and neutral impurity scattering are considered over the entire range of dopant densities and temperatures studied. In addition, the effects of hole–hole (h–h) scattering on lattice and ionized impurity scattering mobilities are also taken into account in mobility formulation. In view of the complex nature of heavy doping effects and the uncertainties in accounting for hole density and impurity density at high dopant densities, we have restricted our present analysis to boron densities up to $3 \times 10^{18}\,\text{cm}^{-3}$ in which the use of Boltzmann statistics and the neglect of the interband scattering process are justifiable[12].

In Section 2 we describe the theoretical approach, presenting the results of effective mass calculations and mobility and resistivity formulations. The appropriate scattering mechanisms for holes are discussed. In Section 3, the theoretical and experimental results are compared and discussed. Section 4 summarizes the main conclusions derived from this work.

2. THEORETICAL APPROACH

In this section we present the result of our calculations of hole effective mass[11], scattering mechanisms, and the mobility and resistivity formulations for p-type silicon. Theoretical expressions for hole mobility are derived by considering contributions from lattice, ionized impurity and neutral impurity scattering. The effects of (h–h) scattering and valence band nonparabolicity are also taken into account in the mobility formulation.

(a) *Valence band and hole effective masses*

The heavy-hole and light-hole bands of silicon have an extremum at $\bar{k} = 0$, and are degenerate there. The constant energy surfaces for this case are warped spheres. The derivation of an expression for a valence band effective mass which incorporates the nonparabolic nature of the individual bands begins with a simplified model of the warped structure based on the work of Kane[13] and Barber[30]. In this model, the heavy-hole band is characterized by holes with an energy independent but direction dependent effective mass, and the light-hole band is characterized by holes with an energy and direction dependent effective mass. The spin–orbit (SO) band is separated at $\bar{k} = 0$ by an energy $\Delta = 0.044\,\text{eV}$, and is characterized by an effective mass which is temperature dependent. Thus, the heavy-hole band is treated as parabolic for the range of temperatures considered in this work, while the light-hole band is parabolic only for very low values of $\bar{k}$. At higher values of $\bar{k}$, the light-hole band has an energy dependent curvature which takes on the same characteristics as the heavy-hole band for energies greater than 0.02 eV.

Based on the above band model, we have calculated the conductivity effective masses and density of states effective masses for holes in each of the three valence bands as reported in Ref. [11]. The values of m_c^* and m_b^* calculated in Ref. [11] for $100 \leq T \leq 400\,\text{K}$ are summarized in Table 1.

(b) *Mobility formulation and scattering mechanisms*

The calculation of mobility of holes in the valence band of silicon may be achieved by considering two alternative simplified models:

(1) The mobility may be evaluated separately in the heavy-hole band, light-hole band, and the (SO) band by considering all appropriate scattering mechanisms, and then the overall hole mobility is evaluated as a weighted average of the one-band mobilities over their individual hole densities in each band.

(2) An expression for a band combined effective mass which incorporates the nonparabolic and warped nature of the valence band structure is obtained in Ref. [11], and this combined effective mass is then included into the mobility formulation. This approach requires the assumption of equal relaxation time constant in each band when computing the total conductivity effective

Table 1. Density of states and conductivity effective masses of holes in p-type silicon for $N_A = 10^{13}\,\text{cm}^{-3}$ and $100 \leq T \leq 400\,\text{K}$[11]

T(K)	100	150	200	250	300	350	400
$m_{b1}^*(m_0)$	0.5503	0.5547	0.5592	0.5638	0.5685	0.5733	0.5782
m_{b2}^*	0.2481	0.3087	0.3527	0.3859	0.4118	0.4332	0.4496
m_{b3}^*	0.0079	0.0248	0.0441	0.0625	0.0790	0.0937	0.1067
m_b^*	0.6570	0.7023	0.7402	0.7723	0.7997	0.8239	0.8444
m_{c1}^*	0.4271	0.4322	0.4375	0.4429	0.4484	0.4541	0.4599
m_{c2}^*	0.3224	0.4191	0.4743	0.5066	0.5231	0.5319	0.5332
m_{c3}^*	0.2399	0.2427	0.2456	0.2486	0.2517	0.2549	0.2582
m_c^*	0.3967	0.4261	0.4438	0.4549	0.4616	0.4661	0.4686

mass for mobility calculations. This is valid only for the lightly-doped case in which lattice scattering dominates.

A comparison of mobility values calculated by using these two methods indicates that the first approach yields a better agreement (by 3–7%) with experimental data over the range of dopant densities and temperatures studied. Thus, only the first approach will be presented here.

We now discuss various scattering mechanisms in p-type silicon, and present the appropriate mobility formulation for each scattering process. Theoretical expressions for the conductivity mobility of holes and resistivity are derived by considering all the possible scattering contributions from lattice (i.e. acoustical and optical phonons), ionized impurity and neutral impurity scattering. In addition, the effects of (h–h) scattering and the nonparabolicity of valence band structure are also taken into account in the mobility calculations. In the present analysis we consider only the intraband scattering processes in the heavy-hole, light-hole, and SO bands for reasons cited previously[12].

Lattice scattering mobility. The published hole conductivity mobility data for lightly-doped p-type silicon exhibits a $T^{-2.3\pm0.2}$ temperature dependence for $150 < T < 400$ K[1–6]. Since acoustical phonon scattering only leads to theoretical mobility following a $T^{-1.5}$ law, additional scattering due to nonpolar optical phonons and the nonparabolicity of valence bands were included to explain this discrepancy[2]. The nonparabolic band structure in the light-hole band plus the temperature dependence of energy band gap lead to a dependence of hole effective masses on temperature in each band, as is shown in Table 1. Theory concerning lattice mobility due to acoustical and optical phonon scattering has been reported by Herring and Vogt[14] for multivalley semiconductors. The reciprocal relaxation time constants for acoustical and optical phonon scattering are given respectively by[14]

$$\tau_{ai}^{-1} = \frac{\sqrt{2}E_1^2 m_{Di}^{*} kT}{\pi\hbar^4 \rho_s u_s^2} E^{1/2} \tag{1}$$

for acoustical phonon scattering,

$$\tau_{oi}^{-1} = \frac{(2m_{Di}^{*})^{3/2} D_0^2}{4\pi\hbar^2 \rho_s k\theta}\left[(n_0+1)(E-k\theta)^{1/2} + n_0(E+k\theta)^{1/2}\right] \tag{2}$$

for optical phonon scattering, and

$$n_0 = 1/[\exp(\theta/T) - 1] \tag{3}$$

is the phonon distribution function.

In eqns (1), (2), the band index, $i = 1$, 2 or 3 denotes the heavy-hole, light-hole, or the SO band, respectively. This notation will be used for other scattering processes as well. The lattice mobility in each of the three valence bands can be calculated from

$$\mu_{Li} = \frac{q\langle\tau_{Li}\rangle}{m_{ci}^{*}}, \tag{4}$$

where

$$\langle\tau_{Li}\rangle = \frac{4}{3\sqrt{\pi}}\int_0^\infty \tau_{Li} x^{3/2} e^{-x}\, dx, \tag{5}$$

and

$$\tau_{Li} = (\tau_{ai}^{-1} + \tau_{oi}^{-1})^{-1} \tag{6}$$

with

$$x = E/kT.$$

The total lattice mobility, based on a 3-band model, can be expressed by:

$$\mu_L = \left[\mu_{L1} + \mu_{L2}\left(\frac{m_{D2}^{*}}{m_{D1}^{*}}\right)^{3/2} + \mu_{L3}\left(\frac{m_{D3}^{*}}{m_{D1}^{*}}\right)^{3/2}\right] \Big/ \left[1 + \left(\frac{m_{D2}^{*}}{m_{D1}^{*}}\right)^{3/2} + \left(\frac{m_{D3}^{*}}{m_{D1}^{*}}\right)^{3/2}\right] \tag{7}$$

where μ_{L1}, μ_{L2} and μ_{L3} are the lattice scattering mobility given by eqn (4) for the heavy-hole, light-hole, and the SO band, respectively. Values of μ_L, calculated from eqn (7) for boron-doped silicon, along with physical constants are listed in Table 2 for $100 \le T \le 400$ K. Note that our calculated lattice mobility values agree well with the published lattice mobility data for p-type silicon[1–6].

Ionized impurity scattering mobility. In pure silicon, the main contribution to carrier mobility comes from lattice scattering. However, as dopant density increases (or temperature decreases), the role of ionized impurity scattering becomes more important. Theories for ionized impurity scattering have been developed previously by Brooks[15] and Herring[16], Conwell and Weisskopf[17]. Brooks and Herring's (B–H) formula has been widely used in mobility calculations for several semiconductors including silicon. The B–H formula can be written as,

$$\mu_{Ii} = \frac{2^{7/2}\epsilon_s^2 m_{Di}^{1/2}(kT)^{3/2}}{\pi^{3/2} q^3 m_{Ci}^{*} N_I G(b_i)} \times 10^{-2} \tag{8}$$

Table 2. Hole lattice mobility as calculated from eqn (7) and lattice scattering constants for boron-doped silicon

T(K)	100	150	200	250	300	350	400
$\mu_L\left(\frac{cm^2}{V\text{-}S}\right)$	5520	2230	1130	720	474	345	274

θ(K)	735	Ref. [1]
E_1(eV)	7.022	present work†
D_0(eV/cm)	5.7×10^8	present work*
ρ_S(g_m/cm^3)	2.329	Ref. [1]
$\mu S\left(\frac{cm}{S}\right)$	9.037×10^5	Ref. [1]

*This value is comparable to Ref. [1].

†This value is adjusted to yield best fit to the published lattice mobility data[2].

where $i = 1, 2, 3$ and

$$G(b_i) = \ln(b_i + 1) - \frac{b_i}{(b_i + 1)}, \tag{9}$$

$$b_i = \frac{24\pi m^*_{Di}\epsilon_s (kT)^2}{q^2\hbar^2 p'} \times 10^{-6}, \tag{10}$$

$$p' \triangleq p + N_A^-(1 - N_A^-/N_A), \text{ for } N_D = 0. \tag{11}$$

The total ionized impurity scattering mobility is calculated from:

$$\mu_I = \left[\mu_{I1} + \mu_{I2}\left(\frac{m^*_{D2}}{m^*_{D1}}\right)^{3/2} + \mu_{I3}\left(\frac{m^*_{D3}}{m^*_{D1}}\right)^{3/2}\right] \Big/ \left[1 + \left(\frac{m^*_{D2}}{m^*_{D1}}\right)^{3/2} + \left(\frac{m^*_{D3}}{m^*_{D1}}\right)^{3/2}\right] \tag{12}$$

where μ_{I1}, μ_{I2} and μ_{I3} are calculated from eqn (8) for the heavy-hole, light-hole. and the SO band, respectively.

Note that eqn (8) does not include such effects as the variation of dielectric constant around the impurity due to a position-dependent screening which may become important for the heavily-doped case. Since we have restricted our analysis for $N_A \leq 3 \times 10^{18}\,\text{cm}^{-3}$, neglecting the aforementioned effect should not introduce an appreciable error in our mobility calculations.

Neutral impurity scattering mobility. Although neutral impurity scattering may not be as important as other scattering mechanisms discussed above in the range of dopant density and temperature considered here, it becomes important at low temperatures or at high dopant densities. For completeness, we have included this scattering mechanism in our mobility formulation. The mobility formula derived by Sclar[19] is employed here for neutral impurity scattering.† Sclar used his calculation of the scattering from a three-dimensional square well to estimate the influence of a weakly bound state on the scattering. From his calculation he obtained:

$$\mu_{Ni} = 0.82\mu_{Ei}\left[\frac{2}{3}\left(\frac{kT}{E_N}\right)^{1/2} + \frac{1}{3}\left(\frac{E_N}{kT}\right)^{1/2}\right] \tag{13}$$

where

$$E_N = 1.136 \times 10^{-19}(m^*_D/m_0)(\epsilon_0/\epsilon_s)^2, \tag{14}$$

and

$$\mu_{Ei} = \frac{2\pi^3 q^3 m^{*2}_D}{5N_N\epsilon_s h^3 m^*_{Ci}} \times 10^{-2}. \tag{15}$$

Equation (15) is the mobility expression derived by Erginsoy[20] for neutral impurity scattering, based on the partial wave expansion approximation.

The total neutral impurity scattering mobility can be computed from:

$$\mu_N = \left[\mu_{N1} + \mu_{N2}\left(\frac{m^*_{D2}}{m^*_{D1}}\right)^{3/2} + \mu_{N3}\left(\frac{m^*_{D3}}{m^*_{D1}}\right)^{3/2}\right] \Big/ \left[1 + \left(\frac{m^*_{D2}}{m^*_{D1}}\right)^{3/2} + \left(\frac{m^*_{D3}}{m^*_{D1}}\right)^{3/2}\right] \tag{16}$$

where μ_{N1}, μ_{N2} and μ_{N3} are calculated from eqn (13).

Effect of hole–hole scattering. The mobility formulas given by eqns (1)–(16) neglect the effect of hole–hole (h–h) scattering. The importance of including (e–e) scattering in n-type silicon has been discussed in detail in our previous paper[21]. In this section the effect of (h–h) scattering in p-type silicon is discussed. The (e–e) and (h–h) scattering events, while not directly producing a change in total momentum, provide a mechanism for the redistribution of momentum gained from the electric field. The maximum effect of (h–h) scattering can be readily calculated (by classical treatment) if the distribution function is Maxwellian and centered about the drift velocity. Assuming $\tau = aE^s$ and by analogy of (e–e) scattering, it can be shown that the ratio of hole mobilities with and without (h–h) scattering is given by[23]:

$$\gamma_{hh} = \frac{\mu_{hh}}{\mu_0} = \frac{\langle v_{hh}\rangle}{\langle v_0\rangle} = \frac{1}{\langle\tau\rangle\langle\tau - 1\rangle} = \Gamma^2(5/2)\left[\Gamma\left(\frac{5}{2} + s\right)\Gamma\left(\frac{5}{2} - s\right)\right]^{-1}. \tag{17}$$

For acoustical phonon scattering with $s = -1/2$, eqn (17) predicts a value for $r_{hh} = 9\pi/32 \triangleq 0.88$, while for ionized impurity scattering $s = 3/2$ and $\gamma_{hh} = 3\pi/32 \triangleq 0.295$.

It is noted that γ_{hh} given by eqn (17) shows no dependence on hole density and temperature. A more rigorous treatment to account for the effect of carrier–carrier scattering on ionized impurity scattering mobility has been developed by Luong and Shaw[22], using a one-particle-like approximation from the Hartree–Fock theory. Applying their (L–S) thoery to the case of (h–h) scattering on ionized impurity scattering, the B–H formula (i.e. eqn (8)) is reduced by a factor which can be expressed in closed form:

$$\gamma_{hhI} = (N_A^-/p')[1 - \exp(-p'/N_A^-)] \tag{18}$$

where N_A^- is the ionized acceptor density, and p' is the screening hole density given by eqn (11).

In contrast to the classical formula (i.e. eqn (17)), eqn (18) predicts a dependence of γ_{hhI} on hole density and hence temperature. Values of γ_{hhI} may vary between 0.432 and 0.632, depending on the degree of ionization of the shallow acceptor impurities.

A comparison of the values, γ_{hhI}, calculated from eqns (17) and (18) indicates that the classical formula (i.e. eqn (17)) overestimates the (h–h) scattering effect. Furthermore, by correcting lattice and ionized impurity scattering mobilities separately the effect of (h–h) scattering may also be overestimated. To overcome these difficulties we have derived a semi-empirical formula, based on eqn (17), to correct the effect of (h–h) scattering

†For reasons discussed in Ref. [21].

on the lattice scattering mobility and retained eqn (18) for correcting the effect of (h–h) scattering on ionized impurity scattering mobility. This will be discussed later.

Hole mobility vs dopant density and temperature. We now discuss the mobility calculations for p-type silicon for dopant densities from 10^{13} to $3\times10^{18}\,cm^{-3}$ and temperatures between 100 and 400 K. The combined hole mobility due to both lattice and ionized impurity scattering contributions is calculated according to the mixed scattering formula[18]:

$$\mu_{LI}=\mu_L\left\{1+X^2\left[Ci(X)\cos X+\sin X\left(Si(X)-\frac{\pi}{2}\right)\right]\right\} \tag{19}$$

and

$$X^2=6\mu_L/\mu_I. \tag{20}$$

Equation (19) is obtained by averaging the reciprocal sum of τ_L^{-1} and τ_I^{-1} over the Maxwellian distribution. Here, $Ci(X)$ and $Si(X)$ are the cosine and sine integrals of X, respectively; μ_L and μ_I are given respectively by eqns (7) and (12) when the effect of (h–h) scattering is neglected. The calculated values of μ_L for $100\le T\le 400$ K are listed in Table 2. The effect of (h–h) scattering can be included, by incorporating the mobility reduction factor, γ_{hh}, given in eqns (17) and (18) into eqn (20) to correct for the values of μ_L and μ_I.

Equation (19) allows the calculations of μ_{LI} for $10^{13}\le N_A\le 3\times10^{18}\,cm^{-3}$, and $100\le T\le 400$ K. When neutral impurity scattering is included, the total mobility may be computed from the expression

$$\mu_P=[\mu_{LI}^{-1}+\mu_N^{-1}]^{-1} \tag{21}$$

where μ_{LI} and μ_N are given by eqns (19) and (16), respectively.

The use of eqn (21) for mobility calculations may be considered as a good approximation here since neutral impurity scattering, being energy independent, does not affect any contributions from μ_L and μ_I. Our calculations of μ_N indicated that contribution from neutral impurity scattering to total hole mobility is less than 10% over the entire range of dopant densities and temperatures studied here. As a result, the error introduced by this approximation is expected to be negligibly small.

The procedure for incorporating the effect of (h–h) scattering on the lattice scattering mobility for p-type silicon is similar to that of n-type silicon[21]. For example, for acoustical phonon scattering, we assume that γ_{hh} decreases linearly with increasing dopant density from $\gamma_{hh}=1$ at $N_A=10^{15}\,cm^{-3}$ to a maximum value of $\gamma_{hh}=9\pi/32\triangleq 0.88$ for $N_A\ge 3\times10^{17}\,cm^{-3}$, as predicted by eqn (17) (i.e. $\gamma_{hh}=1.0004-0.08N_A/2\times10^{17}$ is used in the calculation). This provides the best fit to the experimental data for the range of dopant densities and temperatures studied. This approximation may also offset the possible overestimation of the (h–h) scattering effect by eqn (17) discussed earlier. For ionized impurity scattering, γ_{hhI} is calculated from eqn (18) which is applicable for the entire dopant density and temperature range considered here. The mobility reduction factor for optical phonon scattering is evaluated numerically using eqn (17). For neutral impurity scattering no correction is needed since τ_N is independent of energy.

Resistivity vs dopant density and temperature. The resistivity for p-type silicon is calculated from

$$\rho=\frac{1}{q\mu_p p} \tag{22}$$

where μ_p is the hole mobility given by eqn (21), and the hole density for the nondegenerate case is

$$p=p_1+p_2+p_3=N_v\exp\left(-\frac{E_F-E_V}{kT}\right) \tag{23}$$

where $N_v=2(2\pi m_D^* kT/h^2)^{3/2}$ is the effective density of valence band states, and p_1, p_2 and p_3 are hole densities in the heavy-hole, light-hole and the SO bands, respectively.

In order to calculate hole mobility and resistivity from eqns (21) and (22), it is necessary to know the exact amount of ionized and neutral impurity densities so that individual scattering contributions and hole density can be evaluated. This is done as follows:

The ionized boron densities for boron-doped silicon are computed by solving the charge balance equations for the Fermi energy by the iteration procedure. Since the minority carrier density is negligible, the charge balance equation for uncompensated p-type silicon is simply:†

$$p\simeq N_A^- \tag{24}$$

where[23]

$$N_A^-=\frac{N_A}{1+\left[4+2\exp\left(-\frac{\Delta}{kT}\right)\right]\exp(E_A-E_F)/kT} \tag{25}$$

is the ionized acceptor density, and $\Delta=0.044$ eV for p-type silicon. Equation (25) is used to include the contribution from the SO band.

Experimental evidence indicates that the acceptor ionization energy E_A is not a constant, but decreases with increasing dopant density[24–25]. A study by Penin *et al.*[25] in heavily-doped silicon from 4 to 300 K shows no evidence of an ionization energy for shallow impurities such as phosphorus or boron at impurity densities greater than $3\times10^{18}\,cm^{-3}$. The dependence of ionization energy on dopant density for boron-doped silicon can be expressed by:

$$E_A\triangleq 0.0438-3.037\times10^{-8}N_A^{1/3}. \tag{26}$$

With the help of eqns (23) through (26), the hole

†A more general form of the charge neutrality equation is $N_A^- - N_D^+ = p - n$, which should be used if n and N_D^+ are not negligible compared to p and N_A^-, respectively.

density and fraction of ionized boron density can be calculated as functions of dopant density and temperature.

3. RESULTS AND DISCUSSIONS

Using the theoretical expressions derived in Section 2, we have calculated the hole mobility and resistivity as a function of dopant density and temperature in boron-doped silicon for $10^{13} \leq N_A \leq 3 \times 10^{18}\,cm^{-3}$ and $100 \leq T \leq 400$ K. The results are compared with experimental data. Figure 1 shows the hole mobility plotted as a function of hole density at 300 K for boron-doped silicon. Curve 1 is our theoretical calculation using eqns (1)–(21); curves 2 and 3 are reproduced from Irvin and Sze[8], and Wagner[9], respectively. Note that our calculated mobility values are within 5% of the values reported by Wagner for $N_A \leq 10^{17}\,cm^{-3}$. However, for $N_A > 10^{17}\,cm^{-3}$, our calculated values are substantially higher than those of Wagner[9] (e.g. the deviation is 2.2% at $10^{17}\,cm^{-3}$, and increases to 22.6% at $10^{18}\,cm^{-3}$). To explain this discrepancy, we noted that Wagner[9] obtained an empirical mobility expression based on measurements of boron implanted silicon. The amount of boron retained in the silicon was determined by integration of data obtained from incremental sheet resistance and Hall effect measurements on layers which were sectioned by anodic oxidation. A mobility value as a function of boron density was derived which made the integrated dose equal to the implanted dose. This was done with the assumption that all of the boron was electrically active and ionized. This assumption is valid only at low dopant density or at high temperature where full ionization of boron atoms prevails. For example, our theoretical calculations indicate that at 300 K, $N_A^-/N_A = 0.93$ for $N_A = 10^{17}\,cm^{-3}$, and $N_A^-/N_A = 0.75$ for $N_A = 10^{18}\,cm^{-3}$. Thus, failure to correct this deionization effect at higher dopant density or lower temperature in the mobility calculations would result in a large error in mobility values derived from resistivity measurements.† Curve 3 was reproduced using Caughey and Thomas'[26] empirical formula fitted to the Sze and Irvin's mobility curve[8]. This mobility curve is based on data from Hall effect measurements, which give hole density within the uncertainty of the Hall scattering factor, and on data from chemical techniques which give total dopant density. The lower mobility values shown in curve 3 as compared to Wagner's may be attributed to the fact that Sze and Irvin's mobility curve is based mainly on Ga-doped silicon in the region $10^{16} < N_A < 10^{18}\,cm^{-3}$, which is expected to have a lower mobility value due to the deeper ionization energy of gallium as compared to boron.

From the above analysis, it is clear that values of carrier mobility calculated from measurements of resistivity and dopant density are correct only if the carrier density is equal to the dopant density.

The mobility formulas presented in Section 2 were used to compute the hole mobility as a function of dopant density and temperature for dopant densities between 10^{13} and $3 \times 10^{18}\,cm^{-3}$ and temperatures between 100 and 400 K. The results are displayed in Figs. 2 and 3, respectively. Due to lack of mobility data we were unable to compare between theory and experiment over

†Excellent agreement is obtained between our calculated mobility values and Wagner's for $10^{17} \leq N_A \leq 3 \times 10^{18}$ when deionization effect of boron impurity is taken into account.

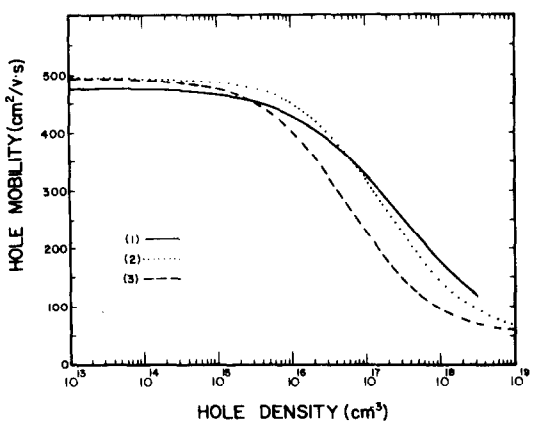

Fig. 1. Hole mobility vs hole density for boron-doped silicon at 300 K. Curve 1 is our theoretical calculations, curve 2 is reproduced from Wagner[9], and curve 3 is from Caughey and Thomas[26]. Curves 2 and 3 are plotted by assuming hole density equal to the dopant density[8, 9], as discussed in the main text.

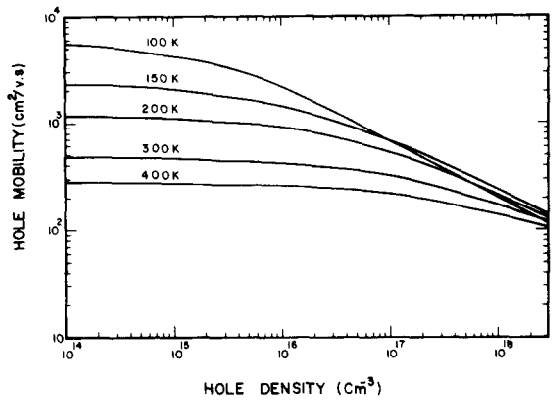

Fig. 2. The calculated hole mobility vs hole density for boron-doped silicon with temperature as a parameter.

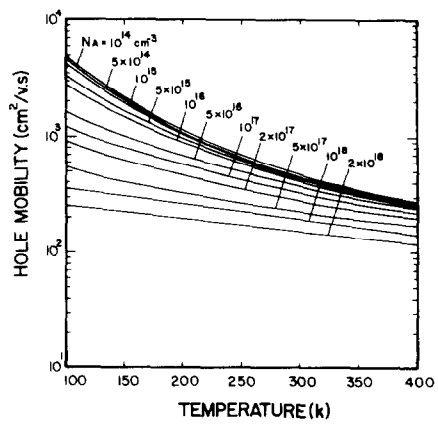

Fig. 3. The calculated hole mobility vs temperature for boron-doped silicon with dopant density as a parameter.

the range of dopant density and temperature reported here.

In order to verify the adequacy of the theoretical model developed in this work, we performed resistivity measurements on nine boron-doped silicon slices with dopant densities ranging from 4.5×10^{14} to $3.2\times10^{18}\,cm^{-3}$ for temperatures between 100 and 400 K, using a planar four probe square array structure as described in our previous paper[21]. The results are compared with our theoretical calculations.

Figure 4 shows the ratio of ionized and total boron impurity density as a function of boron density for $100\le T\le400$ K. It is clearly shown in this figure that the deionization of boron impurities is most significant for $10^{17}<N_A\le3\times10^{18}\,cm^{-3}$ and at low temperatures.

The resistivity for boron-doped silicon is calculated from eqns (21)–(26), and the results are shown in Figs 5–8. Figure 5 shows the plot of resistivity as a function of dopant density for p-type silicon at $T=300$ K. The solid line (curve 1) is our theoretical calculations and solid dots are our experimental data for boron-doped silicon; the dotted curve (curve 3) was reproduced from Irvin's resistivity curve using Caughey and Thomas' empirical formula[26], and the dashed curve (curve 2) is Wagner's for boron-doped silicon[9]. Note that our theoretical calculations agree with Wagner's resistivity data within 6% for $N_A\le3\times10^{18}\,cm^{-3}$ and $T=300$ K. Irvin's resistivity values are higher than both Wagner's and our calculated and measured values for $N_A>10^{16}\,cm^{-3}$. The primary reason for the higher resistivity values is that Irvin's p-type curve is based mainly on Ga-doped silicon for $10^{16}<N_A<10^{18}\,cm^{-3}$. The resistivity measurements on nine boron-doped silicon samples were performed at the National Bureau of Standards, using a planar four probe square array resistor[28]; details of this are described in our previous paper[21] for n-type silicon. It is noted that each data point represents the mean value of resistivity measured over five to seven selected test cells with a maximum variation of resistivity less than 5%. The net dopant density in these specimens was determined by the deep-depletion C–V measurements on MOS test structure adjacent to the four-probe square array resistors. Details of this method can be found elsewhere[28].

To find out the adequacy of our theoretical model for temperatures other than 300 K, we compared the calculated and measured values of resistivity for eight boron-doped silicon samples with N_A ranging from 4.5×10^{14} to $3.2\times10^{18}\,cm^{-3}$ and temperatures from 100 to 400 K. The results show that agreement between our calculated and measured values is within ±6% over the entire range of dopant density and temperature studied, as is evidenced in Fig. 6. Figure 7 displayed our calculated resistivity as a function of temperature for dopant density from 10^{13} to $3\times10^{18}\,cm^{-3}$ in a more regular step. Figure 8 shows the calculated resistivity curves vs dopant density for temperatures between 100 and 400 K. To illustrate the effect of (h–h) scattering on the ionized impurity scattering mobility, we calculate the mobility reduction factor, r_{hhI}, from eqn (18), and the

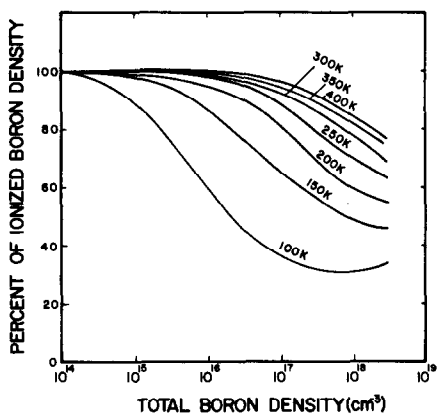

Fig. 4. Theoretical calculations of the ratio of ionized and total boron density vs boron density with temperature as a parameter.

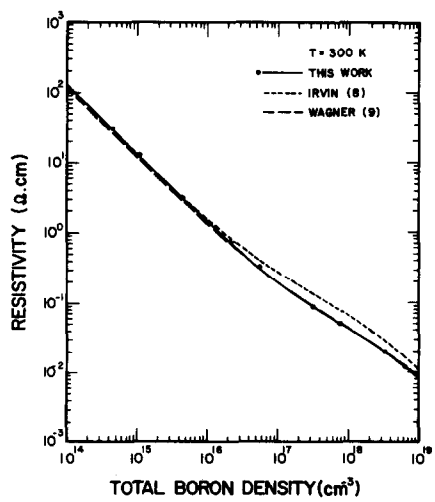

Fig. 5. Resistivity vs dopant density for p-type silicon at 300 K. Solid line is our theoretical calculations, broken line is from Wagner[9] and dotted line is from Irvin[29] which is mainly on Ga-doped silicon for $10^{16}\le N_A\le10^{18}\,cm^{-3}$.

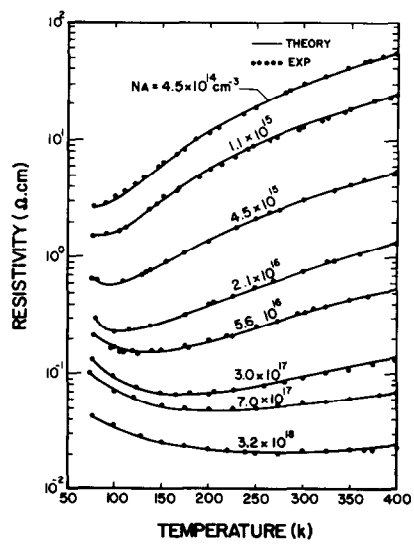

Fig. 6. Resistivity vs temperature for eight boron-doped silicon samples. Solid lines are the theoretical calculations and solid dots are the experimental data taken from NBS-3 four probe square array test structures on these samples[28].

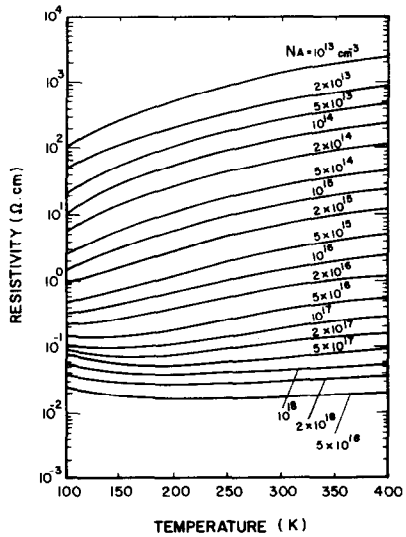

Fig. 7. Theoretical calculations of resistivity vs temperature for boron-doped silicon with dopant density as a parameter.

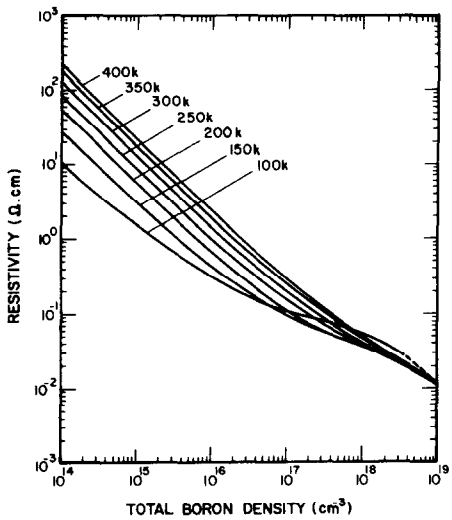

Fig. 8. Theoretical calculations of resistivity vs dopant density for boron-doped silicon with temperature as a parameter.

results are displayed in Fig. 9 for temperatures between 100 and 400 K. The result shows that (h–h) scattering increases with increasing dopant density and decreasing temperature in which the deionization effect becomes more prominant. Finally, it is worth noting that both mobility and resistivity depend more strongly on temperature for the lightly doped case where lattice scattering is dominant and become less temperature dependent for N_A greater than $10^{18}\,cm^{-3}$ where neutral impurity scattering prevails as is shown in Figs. 3 and 8 respectively.

4. CONCLUSIONS

Using a 3-band model, theoretical expressions have been derived to compute hole mobility and resistivity as functions of dopant density and temperature for boron-doped silicon. In addition to considering contributions from scattering by lattice phonons, ionized impurities, and neutral impurities, our model also takes into account the effect of (h–h) scattering on both lattice and ionized impurity scattering mobilities. The nonparabolicity of valence band structure is included in effective mass calculations.

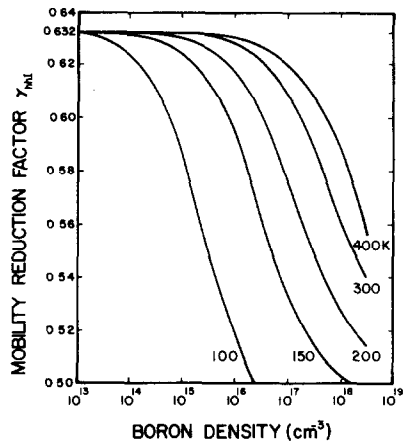

Fig. 9. The mobility reduction factor, γ_{hhl}, as a function of dopant density for boron-doped silicon, for $100 \le T \le 400$ K, showing the effect of (h–h) scattering on ionized impurity scattering mobility as is calculated from eqn (18).

Resistivity analysis for nine boron-doped silicon samples shows that for dopant densities less than $3 \times 10^{18}\,cm^{-3}$, agreement between the calculated and measured values of resistivity is within ±6% for $100 \le T \le 400$ K. A comparison between our calculated mobility values with those of Wagner's data at 300 K shows that agreement is within ±5% for $N_A \le 1.4 \times 10^{17}\,cm^{-3}$ and is increased to about 27% at $N_A = 2.5 \times 10^{18}\,cm^{-3}$. This discrepancy can be eliminated if the effect of deionization of boron impurity were included in Wagner's calculation. From this study, we have found that the theoretical expressions derived in this work are adequate for mobility and resistivity calculations for p-type silicon valid for $10^{13} \le N_A \le 3 \times 10^{18}\,cm$ and $100 \le T \le 400$ K.

It is, however, important to point out that incorporation of the (h–h) scattering as well as deionization effects in the mobility and resistivity calculations play a major role in bringing good agreement between theory and experiment in the range of dopant densities (i.e. $5 \times 10^{16} \le N_A \le 3 \times 10^{18}\,cm^{-3}$) in which existing theories failed.

Our mobility and resistivity calculations also reveal that contribution from SO band is negligible for $T <$ 200 K. Using a 2-band model (i.e. neglecting SO band) in the mobility calculations should not introduce any noticeable error (i.e. less than 5%) over the range of dopant densities and temperatures reported here.

Finally, a rigorous formulation for correcting the effect of (h–h) scattering on lattice and ionized impurity scattering together is needed to further improve our mobility formulations. The extension of the present work to higher dopant densities and lower temperatures is highly desirable.

Acknowledgements—The author would like to express his special thanks to Dr. W. M. Bullis for his critical review of the manuscript and for his valuable comments. He would also like to acknowledge stimulating discussions and assistance on the part of Dr. M. G. Buehler and W. R. Thurber during the course of this study. The planar four-probe test structures used in the present resistivity measurements were fabricated by Y. M. Liu of NBS. R. L. Mattis and W. R. Thurber provided the information of dopant density in these test samples. Thanks are also due to L. C. Linares for effective mass calculations and for checking other theoretical calculations described in this work.

REFERENCES

1. G. Ottaviani, L. Reggiani, C. Canali, F. Nava and A. Alberigi-Quaranta, *Phys. Rev. B.* **12**, 3318 (1975).
2. M. Costato and L. Reggiani, *Il Nuovo Cimento* **68**, 64 (1970).
3. F. J. Morin and J. P. Maita, *Phys. Rev.* **96**, 28 (1954).
4. T. T. Braggins, Ph.D. dissertation, University Microfilms International, Ann Arbor, Michigan (1975).
5. M. Prince, *Phys. Rev.* **93**, 1204 (1954).
6. G. W. Ludwig and R. L. Watters, *Phys. Rev.* **101**, 1699 (1956).
7. N. Sclar, *IEEE Trans. Electron Dev.* **ED-24**, 709 (1977).
8. S. M. Sze and J. C. Irvin, *Solid-St. Electron.* **11**, 599 (1968).
9. S. Wagner, *J. Electrochem. Soc.* **119**, 1570 (1972).
10. K. Y. Tsao and C. T. Sah, *Solid-St. Electron.* **19**, 949 (1976).
11. L. C. Linares and S. S. Li, *Phys. Rev. B.*, to be published (1978).
12. D. M. Brown and R. Bray, *Phys. Rev.* **127**, 1593 (1962).
13. E. O. Kane, *J. Phys. Chem. Solids* **1**, p. 82 (1956).
14. C. Herring and E. Vogt, *Phys. Rev.* **101**, 944 (1956).
15. H. Brooks, *Theory of the Electrical Properties of Germanium and Silicon, Advances in Electronics and Electron Physics* (Edited by L. Marton), Vol. 7, 85–182. Academic Press, New York (1955).
16. C. Herring, *Bell Syst. Tech. J.* **36**, 237 (1955).
17. E. Conwell and V. F. Weisskopf, *Phys. Rev.* **77**, 388 (1950).
18. P. P. Debye and E. M. Conwell, *Phys. Rev.* **93**, 693 (1954).
19. N. Sclar, *Phys. Rev.* **104**, 1559 (1956).
20. C. Erginsoy, *Phys. Rev.* **79**, 1013 (1950).
21. S. S. Li and W. R. Thurber, *Solid-St. Electron.* **20**, 609 (1977); see also S. S. Li, *NBS Special Publication* 400–33, March (1977).
22. M. Luong and A. W. Shaw, *Phys. Rev.* **B4**, 2436 (1971).
23. S. S. Li, *NBS Special Publication* 400–47, to be published (1978).
24. G. L. Pearson and J. Bardeen, *Phys. Rev.* **75**, 865 (1949).
25. N. A. Penin, B. G. Zhurkin and B. A. Volkov, *Sov. Phys.—Solid State* **7**, 2580 (1966).
26. D. M. Caughey and R. E. Thomas, *Proc. IEEE* **55**, 2192 (1967).
27. N. Sclar, *Transc. Elec. Devices* **ED-24**, 709 (1977).
28. M. G. Buehler, *NBS Special Publication* 400–22 (1976); M. G. Buehler and W. R. Thurber, *IEEE Trans. Electron Dev.* **ED-23**, 968 (1976).
29. J. C. Irvin, *Bell Sys. Tech. J.* **16**, 387 (1962).
30. H. D. Barber, *Solid-St. Electron.* **10**, 1039 (1967).